# Citrate Coordination and Bridging of Gold Nanoparticles: The Role of Gold Adatoms in AuNP Ageing

| | |
|---|---|
| Journal: | *ACS Nano* |
| Manuscript ID | nn-2020-03050g.R3 |
| Manuscript Type: | Article |
| Date Submitted by the Author: | 11-Jun-2020 |
| Complete List of Authors: | Grys, David-Benjamin; University of Cambridge, Department of Physics<br>de Nijs, Bart; University of Cambridge, Department of Physics<br>Salmon, Andrew; University of Cambridge, Department of Physics<br>Huang, Junyang; University of Cambridge, Department of Physics<br>Wang, Wenting; University of Cambridge, Department of Physics<br>Chen, Wei-Hsin; University of Cambridge, Department of Physics<br>Scherman, Oren; University of Cambridge, Melville Laboratory for Polymer Synthesis, Department of Chemistry<br>Baumberg, Jeremy; University of Cambridge, Department of Physics |
| | |

# Citrate Coordination and Bridging of Gold Nanoparticles: The Role of Gold Adatoms in AuNP Ageing

*David-Benjamin Grys†, Bart de Nijs†, Andrew R. Salmon†, Junyang Huang†, Wenting Wang†, Wei-Hsin Chen†, Oren A. Scherman‡, Jeremy J. Baumberg†**

† NanoPhotonics Centre, Cavendish Laboratory, Department of Physics, JJ Thompson Avenue, University of Cambridge, Cambridge, CB3 0HE, UK

‡ Melville Laboratory for Polymer Synthesis, Department of Chemistry, University of Cambridge, Lensfield Road, Cambridge CB2 1EW, UK

*E-mail: jjb12@cam.ac.uk

ABSTRACT

Gold nanoparticles used in many types of nanostructure are mostly stabilized by citrate ligands. Fully understanding their dynamic surface chemistry is thus essential for applications, particularly since ageing is frequently a problem. Using surface-enhanced Raman spectroscopy (SERS) in conjunction with density functional theory (DFT) calculations, we are able to determine Au-citrate coordination in liquid with minimal invasiveness. We show that citrate coordination is mostly bidentate and simply controlled by its protonation state. More complex binding motifs are caused by interfering chloride ions and gold adatoms. With increasing age of stored gold nanoparticle suspensions, gold adatoms are found to move atop the Au facets and bind to an additional terminal carboxylate of the citrate. Aged nanoparticles are fully refreshed by removing these adatoms, using etching and subsequent boiling of the gold nanoparticles.

KEYWORDS

nano-gap, colloidal gold, gold atom movement, capping-agent, ligand, SERS reproducibility

Colloidal gold nanoparticles (AuNPs) form a fundamental building block in many applications across nanotechnology as well as underpinning natural science. Over recent decades, the synthesis of gold nanoparticles has been refined to yield diverse shapes, sizes, and coatings.[1-3] Such AuNPs are now utilized in immunoassays, drug-delivery systems, cancer-therapy, catalysis, microscopy, nano-robots, chemical sensing and many more applications.[4-7] Synthesis of the prototypical colloidal system for spherical gold nanoparticles is based on a simple reaction reducing auric acid with either sodium citrate or sodium borohydride. Sodium citrate is particularly interesting as it is cheap, non-toxic, and not only acts as the reducing agent but its negatively-charged carboxylates are also responsible for the charge-stabilization of the AuNPs.

As applications for citrate-capped gold nanoparticles become ever more dependent on their precise surface chemistry, fully understanding the citrate coordination and most crucially time-dependent rearrangements (termed ‘ageing’) on the AuNP surfaces become essential. Previous studies of citrate on metallic nanoparticles use various spectroscopic techniques including attenuated total reflectance infrared (ATR-IR),[8,9] Fourier transform infrared (FTIR),[10] X-ray photoelectron (XPS),[11] solid-state nuclear magnetic resonance (NMR),[12] and surface-enhanced Raman spectroscopy (SERS)[13,14] reporting a wide range of binding motifs (and contradicting each other). As demonstrated below, we believe that this wide disparity of results is caused by the high sensitivity of citrate binding to its chemical environment. In order to provide a more complete picture, it is crucial to take into account time-dependence, pH, cations and anions (specifically chloride) and also the reconstruction of the gold surface itself.

Here, we employ SERS which is advantageous compared to previous techniques (ssNMR, ATR-IR, XPS) as it records the vibrational signatures of citrate anions directly in the liquid state and exclusively at the metal interfaces of colloidal gold nanoparticles. We investigate the effects of benign (Cucurbit[5]uril = CB[5]) and also more invasive (*e.g.* NaCl) aggregating agents on citrate coordination. Our plasma-cleaned AuNP films that mimic colloidal Au clusters without the need for aggregating agents, allow us to record SERS spectra in the absence of chloride and citrate decomposition products.

By this method, we provide strong evidence that the time- and temperature-dependent rearrangement of citrate anions (from $\mu_2$ to $\mu_4$, $c_2$ to $c_2t_2$, see text for details on custom notation) on the AuNP surface (ageing) is driven by migration of Au adatoms on the facet. As we show for CB[5], the increased binding affinity of citrate inhibits ligand-exchange. Aged AuNPs can simply be 'refreshed' by reconstructing the AuNP facets.

With additional parameters (age, pH and ions), we find that it is possible to unify previous results on citrate coordination found in the literature: citrate coordinates in accordance with its protonation state preferring bidentate binding with both carboxylate oxygens over monodentate binding, which is only encountered in environments rich in chloride ions. For pH<6.8 bidentate bridging of the central carboxylate ($\mu_2$-1κO$^1$:2κO$^3$, $c_2$) is dominant whereas only for pH>6.8 are modes of the terminal carboxylates bound independently of the central carboxylate (*e.g.* $\mu_4$-1κO$^{1'}$:2κO$^{3'}$3κO$^{1''}$:4κO$^{3''}$, $t_2t_2$). In nanoparticle clusters with sufficiently small gap sizes, we also see citrate spanning across the nanogaps between neighboring nanoparticles. The presence or absence of the citrate spanning mode is a handy tool to estimate the gap size in AuNP nanoclusters.

## RESULTS AND DISCUSSION

**Observing citrate adatoms – AuNP ageing.** Home-made spherical gold nanoparticles synthesized using the standard Turkevich/Frens protocol serve as the basis of these ageing investigations.[15,16] Stock AuNPs are synthesized to give average diameters of

50±18nm (Figure S1) at pH=3.5±0.1 and stored in three aliquots (50 ml polypropylene centrifuge tubes) at different temperatures, 5±0.5 °C, 18±2 °C and 28±5 °C (Figure 1a, *i*, for detailed AuNP characterisation see Figure S1).

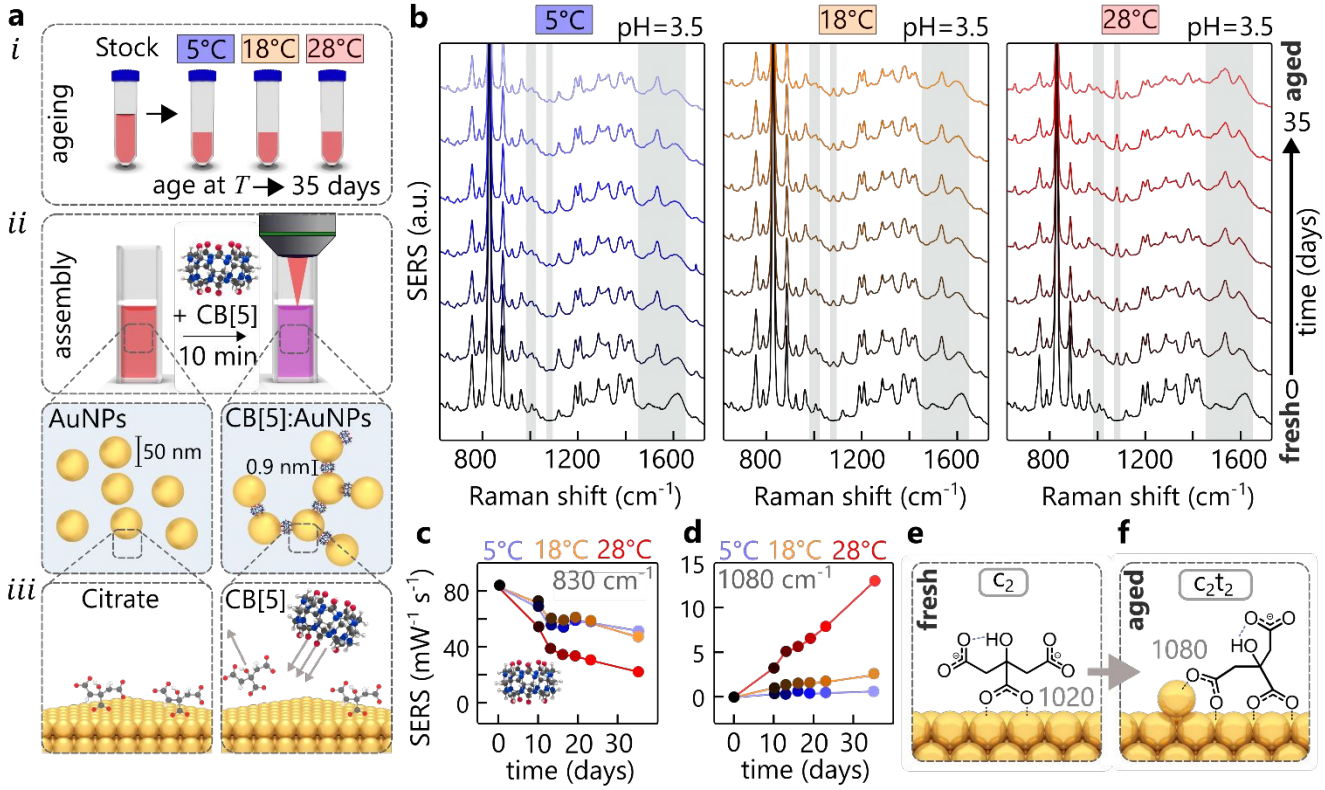


**Figure 1**. Ageing of AuNPs. (a,*i*) Protocol of AuNP ageing; (a,*ii*) Protocol to form CB[5]:AuNP aggregates with precise nanogaps of 0.9 nm; (a,*iii*) Depiction of CB[5] binding onto AuNP surface displacing some of the citrate anions. (b) Ageing experiment over 35 days showing SERS spectra of AuNP:CB[5] aggregates for AuNPs previously stored at 5, 18 and 28°C. (c) Extracted CB[5] signature peak at 830 $cm^{-1}$ (ring breathing mode). (d) Extracted citrate $c_2t_2$ peak at 1080 $cm^{-1}$ for different temperatures in (b), normalized to CB[5] signature peak. (e,f) Proposed citrate coordination in CB[5]:AuNP aggregates for fresh and aged AuNPs, showing influence of thermally-activated Au adatoms.

To probe the surface chemistry using SERS, the gold nanoparticles are aggregated into clusters with the help of the linker molecule cucurbit[5]uril (CB[5]), which acts as a precise molecular spacer (Figure 1a,*ii*, see Figure S2 for alternative salt aggregation).[17] A key advantage in employing CB[5] (instead of a salt) is the highly reproducible SERS spectra, which allow quantitative interpretation (such as calculating activation energies, Figure S3). The CB[5] molecules connect adjacent nanoparticles by displacing citrate (Figure 1a,*iii*) and binding to the gold surface *via* their carbonyl-rimmed portals.[18] Any subtle change of the nanoparticle surface chemistry is directly reflected in the SERS spectra.

Over the course of 35 d, ageing of the AuNPs, SERS spectra of freshly clustered CB[5]:AuNPs are taken after exactly 10 min of aggregation time, giving different spectra for the three aliquots stored at different temperatures (Figure 1b). Despite the excellent short-term reproducibility (<2%) of CB[5]:AuNP aggregates (Figure S4), the overall CB[5] signal diminishes, as tracked by the CB[5] signature peak at 830 $cm^{-1}$ (Figure 1c). The peak intensity drops by a half for $T$=5,18 °C, and even more for $T$=28 °C to a quarter after 30 d. Concurrently, a range of peaks emerge, which are not related to the CB[5] molecule. These vibrations at 995, 1020, 1080, 1385, 1535, 1585 and 1604 $cm^{-1}$ are ascribed to the presence of citrate anions on the gold surface inside the nanogaps (see DFT in Figure S5 and S6). The temporal evolution of these peaks suggests that citrate anions undergo temperature-dependent conformational changes (termed ageing) which partially inhibits CB[5] binding.

Aggregates formed from AuNPs stored at $T$=28°C give rise to a strongly increasing 1080 $cm^{-1}$ vibration with ageing (Figure 1d). This comes from the ν(CC) stretch (see DFT in Figure S6) and appears at this position only if the central (c) and terminal (t) carboxylates are both bound ($c_2t_2$) to the same gold facet, forming a ring (Figure 1f). Here the subscript 2 indicates that a carboxylate has bidentate ($\mu_2$-1κ$O^1$:2κ$O^3$) binding (Figure 1e), with monodentate binding (1κ$O^1$) given subscript 1 (see Figure S8 for kappa/mu convention naming scheme). This linear growth of the $c_2t_2$ binding is much slower at lower

temperature, allowing extraction of its activation energy ~$1.1 \pm 0.2$ eV (see Figure S3). This strongly suggests that $c_2t_2$ binding can only occur upon reconstruction of the Au surface through adatoms, which possess similar calculated and measured activation energies on gold.[19,20] The emergence of the citrate-adatom peaks after ageing shows that CB[5] molecules are no longer able to displace the citrate from the surface due its greater (double) bidentate binding affinity. Eventually, this leads to loss of aggregation and changes in other AuNP chemistries. The timescales involved in this ageing also match those for Au adatom formation and migration under ambient conditions, which explains for instance the need for refrigerated storage of SERS substrates (as for Klarite™).[21] In order to rule out other effects, we investigate the role of monovalent cations and thermal decomposition of citrate by-products. Repeating the ageing experiment with nanoparticles synthesized with heavier $K^+$ cations instead of $Na^+$ yields exactly the same result (see Figure S7). The lack of any shifts in vibrational energies implies the role of cations can be neglected, as also suggested by computational studies.[22]

The SERS spectra of the citrate by-products acetone-dicarboxylate (ADC), acetoacetate (AA), acetate and acetone do not match the peaks emerging in the ageing experiments (see Figure S8). Such by-products are formed during the AuNP reaction as citrate is consumed and also after the reaction through thermal decomposition. The activation energies for the thermal decomposition of ADC[23] and AA[24] are similar to the adatom activation energy. However, rapid decomposition through decarboxylation occurs within a few minutes to a maximum of a few days after AuNP synthesis (see Table S1 for rate calculations).[25] Gold nanoparticles synthesized directly from ADC do not resemble the ageing peaks (see Figure S9). Swapping the supernatant between fresh and aged nanoparticles neither ages the fresh, nor refreshes the aged particles. Finally, in a by-product-free environment, the adatom-driven effect can also be reproduced (see section 4). It is thus implausible that the ageing effects are caused by any citrate by-products.

**Citrate-bound adatoms: reactivation *via* 're-faceting'.** Having shown strong evidence that Au adatoms control the chemical changes in ligand binding, we demonstrate how to reverse this ageing by etching the AuNPs with a strong oxidizing agent such as auric chloride ($HAuCl_4$). This procedure removes weakly-bound gold atoms from edges, steps and vertices[26,27] and therefore can attack gold adatoms coordinated to citrate anions (Figure 2a).

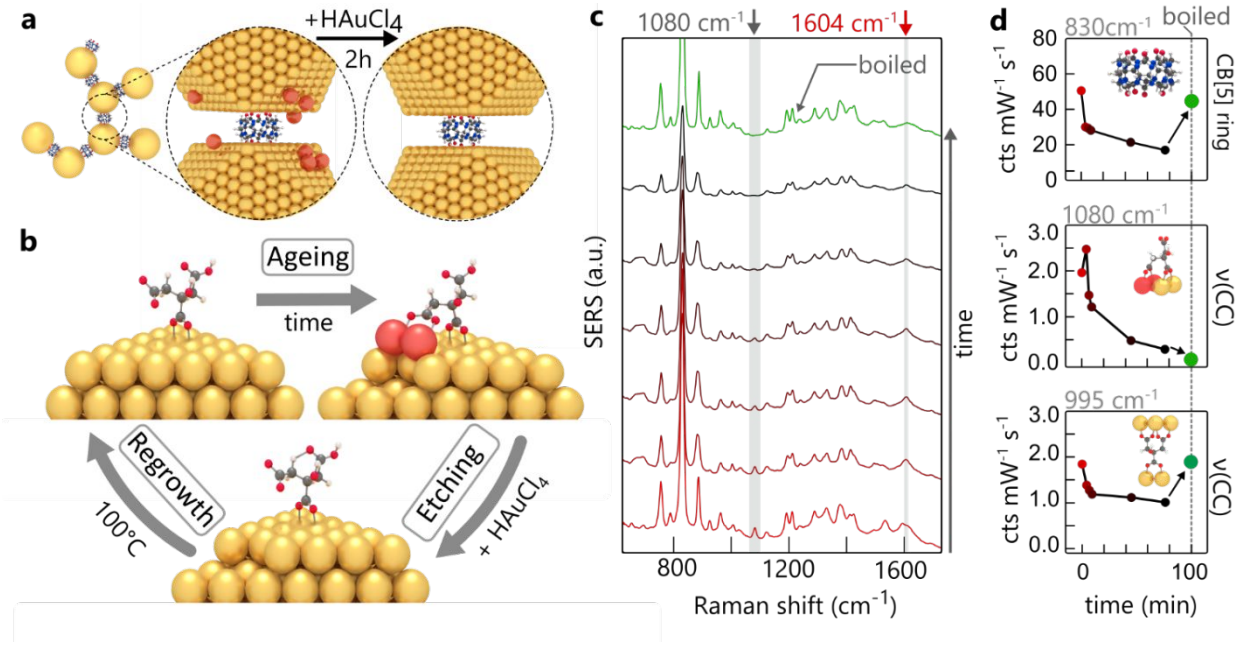


**Figure 2.** Refreshing gold nanoparticles. (a) Ageing by adatoms (red) is reversed by adding $HAuCl_4$ to preformed CB[5]:AuNP aggregates assembled from aged AuNPs, followed by boiling for 5 min. (b) Model of ageing/reversal process showing changing citrate coordination. (c) *In Situ* time-dependent monitoring of SERS spectra during auric chloride etching (reactivation), with (d) SERS strengths from CB[5], 1080 $cm^{-1}$ adatom and 995 $cm^{-1}$ gap-spanning citrate peaks.

To monitor the etching process *In Situ*, CB[5]-bound aggregates are formed over 10 min using aged gold nanoparticles. After aggregation, facet etching is initiated through addition of chloroauric acid to a final concentration of 125 μM. Since the acid is added to

the AuNPs at room temperature, the presence of citrate does not induce nucleation or significant growth (see Figure S10), as is the case during NP synthesis. The *In Situ* SERS spectra (Figure 2b) resolve citrate peaks showing rapid adatom removal through the disappearance of the 1080 $cm^{-1}$ v(CC) bidentate binding (Figure 2c). Detachment of the terminal carboxylates from adjacent AuNPs is also seen as the decay of citrate vibrations v(CC)=995 $cm^{-1}$, $v_a$(COO)=1535 $cm^{-1}$ and $v_a$(COO)=1585 $cm^{-1}$. The persisting $v_a$(COO)=1604 $cm^{-1}$ vibration (Figure 2c, red arrow) shows that the central carboxylate remains bound ($c_2$).

Subsequent boiling in the presence of citrate anneals and reconstructs the etched facets, restoring the CB[5] SERS peak. The unbound terminal carboxylates again bind to the surface of the adjacent AuNP giving terminal-spanning bound citrate but without evidence of any adatoms. The restored AuNP aggregates now behave with the same SERS sensing capability as previously observed. The control measurement, boiling aged AuNPs without adding $HAuCl_4$, leads to an increase of citrate adatom signals (see Figure S11).

**Citrate coordination in the nanogap.** From this understanding of ageing as adatom-induced reconfiguration of citrate anions on gold facets, the general configuration of citrate ions inside nanogaps formed between adjacent nanoparticles can be investigated, both for fresh and aged nanoparticles.

To determine more carefully the citrate configurations inside smaller nanogaps, aggregates are instead formed by salting (reducing the screening length) using either concentrated sodium chloride (NaCl) or trisodium citrate (TSC) buffer solution with pH matching that of the nanoparticle suspension. For freshly made AuNPs aggregated with TSC, the SERS spectra (Figure 3a*,i*) reveal coordination only *via* the central carboxylate ($c_2$, red, bonds in Figure 3b). With full protonation of the non-surface-bound terminal carboxylates at pH=3.5, neighboring citrate anions should form carboxylic acid dimers

(seen in characteristic dimer vibrations at 1700-1715 $cm^{-1}$, see Figure S4), which are only weakly Raman active.[28]

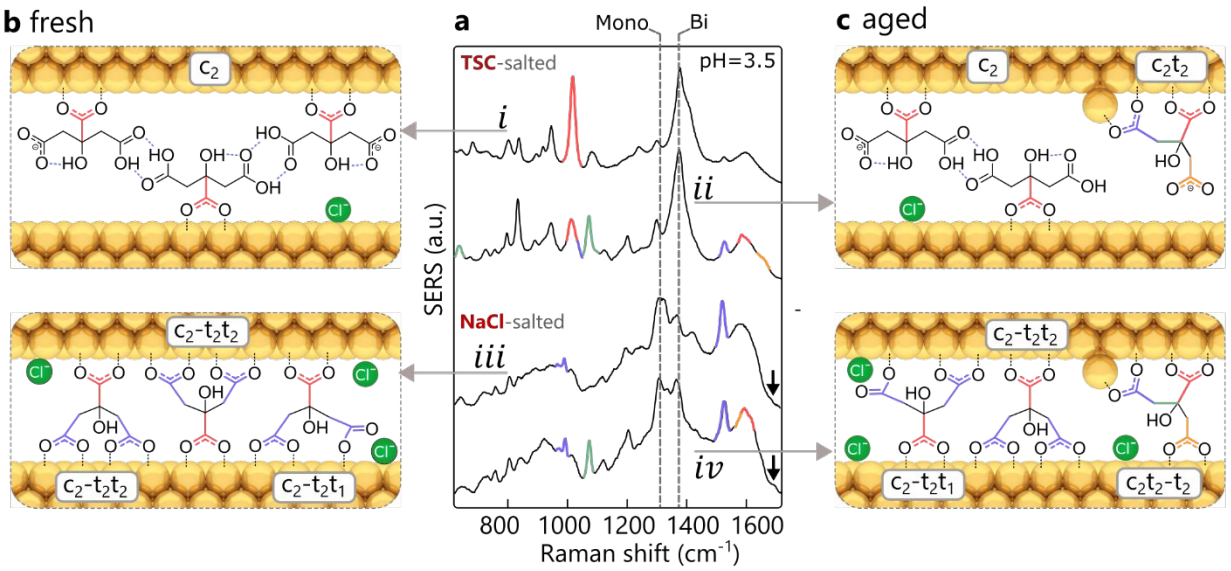


**Figure 3.** Citrate coordination in nanogaps. (a) SERS signals for both aggregation agents at pH=3.5, using fresh and aged AuNPs. (b,c) Proposed models of citrate coordination inside nanogaps in AuNP aggregates for (b) freshly-made, or (c) aged nanoparticles, formed using excess of trisodium citrate (top) or sodium chloride (bottom).

Forming fresh AuNP aggregates instead with excess NaCl generates a different spectrum (Figure 3a,*iii*) in which the dominant citrate mode changes from $c_2$ to the gap-spanning $c_2$-$t_2t_2$ (995 $cm^{-1}$) (blue, bonds in Figure 3b). Here the dash (-) separates groups bound to different nanoparticle surfaces. In addition to the centrally-bound carboxylate, the two terminal carboxylates also coordinate with the neighboring nanoparticle whilst spanning the nanogap (nanogap size estimate is 0.8 to 1.0 nm, see Figure S12). For this to occur, the citrate surface coverage needs to be low enough to allow access to the Au surface. For TSC-salted aggregates, addition of excess citrate instantaneously increases the surface coverage so that spanning cannot happen due to steric crowding, in contrast to NaCl aggregation. In addition to citrate rearrangement with NaCl, a distinct shift from bidentate to monodentate coordination is observed *via* the increasing C-O-Au stretch[29] at

~1300 $cm^{-1}$ (dashed vertical line) together with the decreasing 1385 $cm^{-1}$ symmetric $COO^-$-Au stretch, as well as the emerging 1680 $cm^{-1}$ C=O stretch of the unbound oxygen (black arrow). We speculate that addition of chloride anions near the gold surface (as surface chlorides) prevents citrate from bidentate binding.[30-32] Low-wavenumber vibrations ascribed to Au-Cl bonds indicate the presence of adsorbed chloride on the Au surface (see Figure S13).[33,34] Further control measurements using salts containing mono- or divalent anions with and without chloride ions ($MgCl_2$, $CaCl_2$, Na acetate, Mg citrate) confirm this hypothesis (see Figure S14).

Using aged nanoparticles with TSC (Figure 3a,$ii$), the characteristic $\nu$(CC) vibration at 1080 $cm^{-1}$ (marked in green, with bond in Figure 3c) clearly shows the adatom-induced $c_2t_2$ mode. The shoulder around 1630 $cm^{-1}$ (orange, $ii$) for deprotonated carboxylates, likely stems from the dangling terminal carboxylate of the $c_2t_2$ mode. Evidence is again seen for intermolecular hydrogen-bonding *via* the carboxylic dimer formation (1700-1710 $cm^{-1}$) between $c_2$ citrates. Using NaCl-salted aged AuNP aggregates (Figure 3a,$iv$) gives very similar SERS spectra to the fresh AuNPs, apart from the adatom-induced $c_2t_2$ mode (green). An additional asymmetric carboxylate-Au stretch at 1585 $cm^{-1}$ suggests that the adatom-coordinated citrate can also span the nanogap (orange, $iv$). This is supported by the disappearance of the shoulder at ~1630 $cm^{-1}$ related to strain. Furthermore, loss of the 1020 $cm^{-1}$ peak suggests that both (c,t) carboxylates are now fully coordinated. Evidence for monodentate binding from peaks at 1300 $cm^{-1}$ and 1680 $cm^{-1}$ again suggests chloride ions interfere with bidentate binding.

Results for fresh and aged AuNPs buffered at higher pH values (most commercial NPs are stabilized close to pH=7) suggest that more citrate coordination modes are present (Figure S2 and Table S1).

**Citrate coordination in AuNP films.** Salting of gold nanoparticles is thus invasive since it clearly changes how citrate is coordinated to the gold nanoparticle surface. To

determine the intrinsic citrate signals, an alternative SERS substrate is employed consisting of 1-3 layers of close-packed nanoparticles. To remove all ligands (polymers, citrate, and all decomposition products) from the commercially-synthesized nanoparticles employed, these substrates are $O_2$ plasma cleaned for 30 min. From the SEM images (Figure 4a, close-up in insets and Figure S15) it is evident that the AuNP shape remains intact and no bridges between particles are formed after treatment.[35] Comparing SERS measurements before and after the plasma treatment (Figure 4b) shows all organic compounds are removed from the films (red line), with only a layer of hydroxyl groups left on the surface (giving the low $\upsilon$(Au-OH)= 590 $cm^{-1}$ peak).

After immersing the treated films for 24 h in TSC solution, SERS spectra are taken with a droplet of the TSC solution left on the surface to maintain a similar environment as for the suspended aggregates. To investigate the pH-dependence of citrate binding, a pH series between 1.4 and 8.3 is prepared by immersing the films in mixtures of TSC and citric acid. The SERS spectra (Figure 4c, $i$) resemble those of the TSC-salted colloidal aggregates (as compared to Figure S4). The absence of 1300 and 1680 $cm^{-1}$ peaks implies that coordination is purely through bidentate bridging. Again, the addition of chloride ions to the AuNP films instantaneously generates some monodentate coordination as for colloidal aggregates salted with NaCl (see Figure S16).

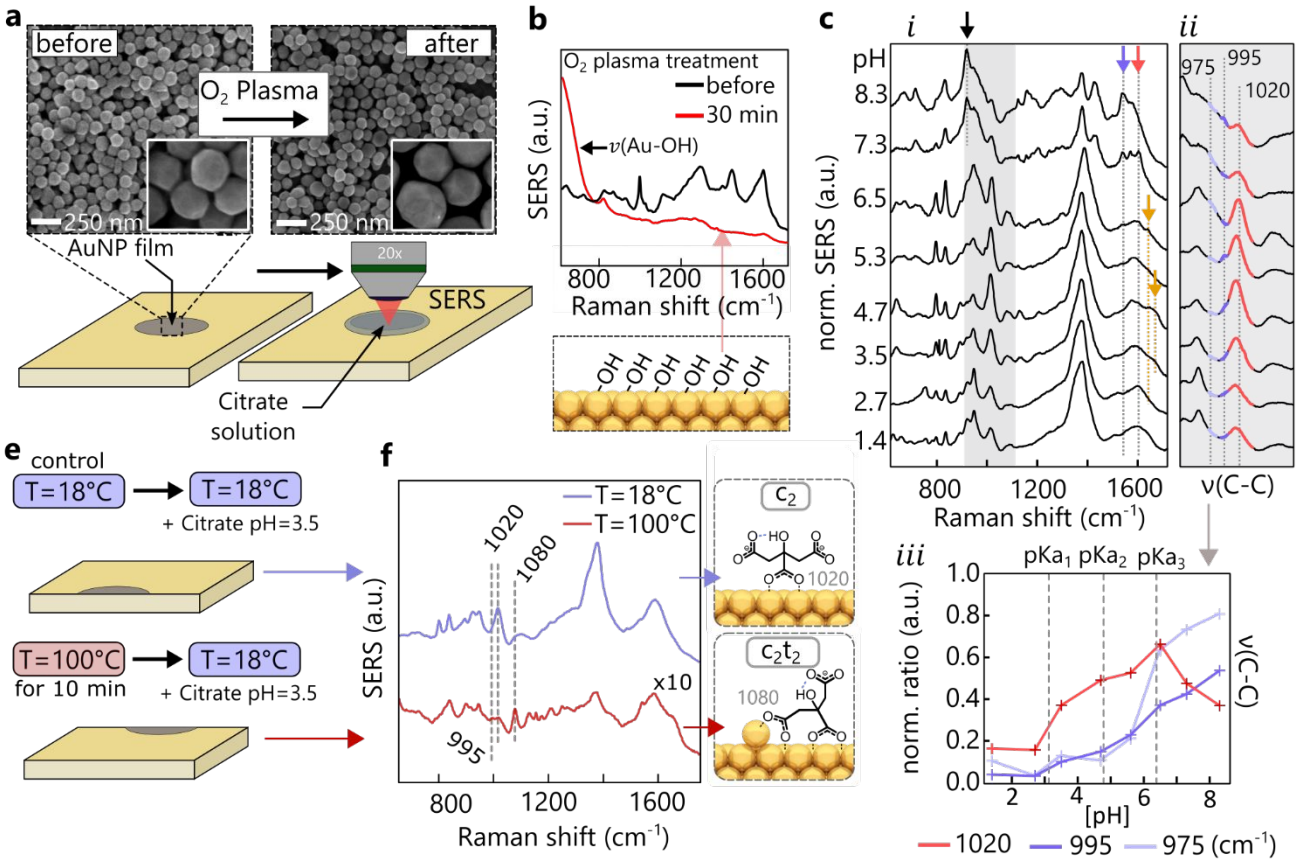


**Figure 4.** Organic-stripped AuNP films. (a) SEM images of AuNP films before and after $O_2$ plasma treatment with insets showing close-ups. (b) SERS spectra before and after $O_2$ plasma treatment, evidencing ligand removal and OH layer (from ambient moisture). (c) (*i*) SERS spectra normalized to symmetric carboxylate stretch at ~1380 $cm^{-1}$ from treated AuNP films with added citrate *vs* pH, together with (*ii*) details of $\nu$(CC) peak, and (*iii*) peak ratios. (e) Experimental protocol of accelerated ageing, showing heating of AuNP films directly after $O_2$ plasma cleaning leads to formation of adatoms, (f) seen in resulting SERS spectra. Heated films resemble adatom response of aged colloidal AuNPs.

Tracking the CC stretches (Figure 4c *ii, iii*) shows that the citrate coordination modes reflect the protonation states of citrate set by its three pKa values at 3.13 (central carboxylate), 4.76 and 6.39 (terminal carboxylates).[36] Below pH=6.5 citrate binding is

again dominated by the 1020 $cm^{-1}$ vibration and therefore the $c_2$ mode (Figure 4c, *ii, iii*, red). There is evidence of dangling carboxylates for 3.5<pH<5.3 (Figure 4c *i*, orange arrow), but the absence of a strong 1080 $cm^{-1}$ vibration suggest that the adatom-driven mode $c_2t_2$ is not present. Instead with a further increase of pH, spanning of the nano gap with the modes $c_2$-$t_2$ and $c_2$-$t_2t_2$ occurs, as seen by the emerging vibrations at 975 $cm^{-1}$ (light blue) and 995 $cm^{-1}$ (dark blue). Above pH=6.5 (where most commercial NPs are stabilized) a decrease of 1020 $cm^{-1}$ and steep increase of 975 $cm^{-1}$ vibrations is observed. Along with the loss of the central (red arrow) and gain of the terminal (blue arrow) asymmetric $COO^-$-Au stretches, additional citrate binding with only the terminal carboxylates is found. (Figure 4c *i*). The strong v($CCOO^-$) mode (black arrow) at 925 $cm^{-1}$ related to the unbound central carboxylate is only present for $t_2t_2$ coordination.

**Ageing in AuNP films**. There are two separate pathways for the ageing of AuNP films and suspensions. For aged AuNP films with their close-packed AuNPs (pH=3.5, 18 °C), the citrate anions preferentially span the gap ($c_2$-$t_2t_2$) with both terminal carboxylates (Figure S17). This is different to ageing of suspended individual AuNPs where spanning cannot occur. Instead, migrating adatoms attract one of the terminal carboxylates to form the $c_2t_2$ mode. After aggregation, the $c_2t_2$ mode can then transition to $c_2t_2$-$t_2$ inside the nanogaps depending on the gap size.

In order to observe the $c_2t_2$ mode in AuNP films, adatoms have to be generated before the films are immersed in TSC solution. This is achieved by heating a plasma-cleaned film to ~100°C for ten minutes (Figure 4e). After cooling to room temperature, control and heated films are immersed in the same TSC solution for 24 h. The SERS spectra from the heated AuNP films (Figure 4f) resemble those of aged colloidal aggregates, showing the $c_2t_2$ modes together with $c_2$-$t_2t_2$. The control sample exhibits only the usual $c_2$ mode as expected for pH=3.5. This shows that a detailed understanding of the citrate binding

modalities and the SERS peaks produced allows a full reconstruction and control of the citrate ligands on gold.

**Overview of adatom experiments.** A summary of experiments supporting the adatom-driven reconfiguration of citrate anions on the AuNP surface, is shown in Table 1. It contains the name of each experiment, the parameters that have been controlled, the experimental conditions and its key results. To make it easier for the reader to find the data, we have added references to the corresponding Figures in the main text and also supporting information.

| Experiment | Parameter | Conditions | Key results | Figure |
|---|---|---|---|---|
| *AuNP:CB[5] ageing* | time | 0 to 35 days ageing | adatom signals emerge over time | 1 |
| *AuNP:CB[5] ageing* | cations time | trisodium ($Na^+$) *vs* tripotassium ($K^+$) citrate AuNPs | same adatom signals over time, no influence of cations | S7 |
| *AuNPs salted (NaCl, TSC) ageing* | time pH | 5mM, citrate-buffered pH=3.8,5.5, 6.8 | adatom signals observed, less intense for higher pH | S2 |
| *SERS of decomposition products* | - | AuNP film *vs* suspension | peak positions not related to citrate adatoms | S8 |
| *acetone-dicarboxylate AuNPs* | - | fresh *vs* aged | peak positions not related to citrate adatoms | S9 |
| *AuNP boiling with $HAuCl_4$* | - | pH=3.5 (before addition of $HAuCl_4$) | ageing peaks removed | 2 |
| *AuNP boiling* | - | pH=3.5 | ageing peaks intensify | S11 |

| | | | | |
|---|---|---|---|---|
| *without $HAuCl_4$* | | | | |
| *AuNP film accelerated ageing* | - | film heated to T=100 °C, then exposed to TSC solution | adatom peaks same as in solution | 4(e,f) |
| *AuNP film ageing* | time | 0 to 87 days | adatom peaks not observed, but citrate bridges AuNPs | S17 |

**Table 1.** Summary of experiments carried-out to support the hypothesis of citrate reconfiguration driven by the formation of gold adatoms.

## CONCLUSION

Our analysis of the SERS of colloidal gold in liquid provides a nuanced account of the complexity of citrate binding to Au, which has previously led to a wide variety of interpretations. By analyzing multiple parameters such as pH, time-dependence (ageing), and the influence of the chemical environment (chloride), we are able to provide a complete picture of citrate coordination.

We show that the dominant coordination mode of citrate (pH<6.8) is the bidentate bridging of the central carboxylate ($c_2$). For even higher pH values (>6.8), unbound central carboxylates can be seen. We prove that surface-bound citrate anions almost exclusively prefer bidentate over monodentate binding. Only in a chloride-rich environment, is monodentate binding present. For citrate trapped inside sub-nm gaps, citrate molecules can be observed to span across the nanogap whilst coordinating all three carboxylates in either the $c_2$-$t_2t_2$ or $c_2t_2$-$t_2$ modes for fresh or aged nanoparticles respectively.

With increasing age of stored gold nanoparticle suspensions, gold adatoms move atop the Au facets and bind to one of the terminal carboxylates yielding the double bidentate bridging mode ($c_2t_2$). These are rather stable, making citrate difficult to remove or undergo

surface diffusion. We find that the adatom signals are independent of monovalent cations ($K^+$ *vs* $Na^+$) and also of citrate decomposition products present in solution. To what extent the adatom-citrate complex and its formation kinetics depend on the type of surface facets is still an open question.

Aged nanoparticles can be fully refreshed by removing these adatoms, using etching and subsequent boiling of the gold nanoparticles. Our demonstration that Au adatoms play a crucial role gives much better control of their utilization for sensing and other nano-assembly-based technologies. This is crucial for widespread adoption in new generations of functional materials and devices.

## EXPERIMENTAL METHODS

**AuNP synthesis.** Sodium citrate tribasic dihydrate, potassium citrate tribasic monohydrate, lithium citrate tribasic tetrahydrate and tetrachloroauric(III) acid trihydrate of analytical grade were purchased from Merck/Sigma Aldrich. To yield particles with an average diameter of ~50 nm, a gold/citrate ratio of 1.33 is employed. 2.28 mL of a 152 mM solution of citrate was added to 150 mL of a 0.38 mM chloroauric acid solution under reflux with under vigorous stirring. Reflux was continued for a further 15 minutes after the after the citrate addition. The resulting wine-red suspension was allowed to cool to room-temperature for one hour.

**AuNP films.** For the AuNP films, 80 nm diameter commercial gold nanoparticles from BBI Solutions were purchased directly from the manufacturer. A total volume of 1 mL with equal parts of chloroform and the AuNP suspension were added to an Eppendorf tube forming a two phase system. After the addition of 150 µL of 1M NaCl, the Eppendorf tube was shaken for ten seconds. In this step, the majority of the nanoparticles are pushed to the interface of the aqueous phase. The supernatant is replaced three times with DI water to wash the particles. The supernatant/DI water was then almost fully removed yielding a

small droplet of concentrated AuNPs at the chloroform/water interface. Subsequently, the droplet was transferred onto an evaporated gold silicon wafer substrate. After the water fully evaporated, the films were washed with DI water and then oxygen plasma cleaned for 30 minutes using a Diener electronic GmbH & Co. KG plasma etcher. Lastly, the films were immersed in the analyte of interest for 24h.

**SERS/Raman measurements.** All Raman and SERS measurements used a Renishaw inVia Raman instrument. The excitation source is a 785 nm infrared laser with 147 mW of laser power available at the objective. For solution measurements, the focal plane of the 5x objective was always set to slightly below the air/liquid interface by maximizing the counts through a z-axis scan. Each solution spectrum was taken with full laser power and ten seconds integration time (if not otherwise stated) and integrated over three acquisitions. For the measurements of AuNP films, a 20x objective was focused using an imaging camera. The integration time was set to ten seconds and three acquisitions taken, with the laser power limited to 0.5% of full power. Liquid measurements were performed using polypropylene 96-well plates with 340 µL capacity per well.

**AuNP aggregate preparation.** For the formation of CB[5]:AuNP aggregates, 6.3 µL of a 125 µM solution of CB[5], synthesized and separated according to the protocol mentioned by Barrow *et al.*[37] was added to 333 µL of the home-made nanoparticles. Exactly ten minutes was allowed for nanoclusters to form before taking SERS spectra. Salted nanoparticles were prepared by using 30 µL of 0.5 M NaCl solution or 1 M citrate solution. For the pH experiments, the pH of the citrate solution was adjusted by mixing 1 M trisodium citrate and 1 M citric acid.

**DFT calculations.** Geometry optimization and frequency calculation were performed using the hybrid functional PBE0 (PBE1PBE) with the 6-311++G(d,p) basis set and the Los Alamos ECP double-zeta basis set for Au atoms and clusters.[38] Solvent effects were considered using the polarizable continuum model (PCM) solvation model. For all calculations the Gaussian 09 *ab-initio* software suite was employed.[39] The Raman

intensities were corrected for the uniform polarizability in the plasmonic gaps. This is achieved by extracting the polarizability tensors from the Gaussian output file and recalculating the intensities.[40]

## ASSOCIATED CONTENT

**Supporting Information**. Additional Figures S1-S17 and Tables S1-S3 are available in the supporting information file (PDF): Characterization of in-house AuNPs, salted AuNPs fresh *vs* aged for different pH, activation energy of adatom mode, CB[5] *vs* salted AuNP aggregates, aqueous *vs* adsorbed citrate, citrate DFT calculations, ageing with $K_3$Citrate AuNPs, spectra of decomposition products, disodium acetone-dicarboxylate AuNPs, etched AuNPs zeta size measurement, boiling aged AuNP aggregates, DFT gap size calculation, chlorides in salted AuNPs, trisodium citrate-salted AuNPs and chlorides, SEM images of AuNP films, AuNP films with TSC and added NaCl, Ageing of AuNP films, extracted citrate coordination modes for salted AuNPs, acetone-dicarboxylic acid decomposition, acetoacetic acid decomposition.

This material is available free of charge *via* the Internet at http://pubs.acs.org.

## AUTHOR INFORMATION

### Corresponding Author

*E-mail: jjb12@cam.ac.uk

### Notes

Source data can be found at https://doi.org/10.17863/CAM.53701

## ACKNOWLEDGMENTS

We acknowledge financial support from EPSRC Grants (EP/L027151/1 and EP/L015889/1). B.d.Nijs acknowledges support from the Leverhulme Trust, the Isaac Newton Trust and support from the Winton Foundation for the Physics of Sustainability. We greatly appreciate useful discussions with C. Jones (BBI).

REFERENCES

(1) Kumar, P. S.; Pastoriza-Santos, I.; Rodriguez-Gonzalez, B.; de Abajo, F. J. G.; Liz-Marzan, L. M. High-Yield Synthesis and Optical Response of Gold Nanostars. *Nanotechnology* **2008**, *19,* 1–6.

(2) Murphy, C. J.; Gole, A. M.; Hunyadi, S. E.; Stone, J. W.; Sisco, P. N.; Alkilany, A.; Kinard, B. E.; Hankins, P. Chemical Sensing and Imaging with Metallic Nanorods. *Chem. Commun.* **2008**, No. 5, 544–557.

(3) Mine, E.; Yamada, A.; Kobayashi, Y.; Konno, M.; Liz-Marzán, L. M. Direct Coating of Gold Nanoparticles with Silica by a Seeded Polymerization Technique. *J. Colloid Interface Sci.* **2003**, *264*, 385–390.

(4) Liu, X.; Dai, Q.; Austin, L.; Coutts, J.; Knowles, G.; Zou, J.; Chen, H. A One-Step Homogeneous Immunoassay for Cancer Biomarker Detection Using Gold Nanoparticle Probes Coupled with Dynamic Light Scattering. *J. Am. Chem. Soc.* **2008**, *130*, 2780–2782.

(5) Douglas, S. M.; Bachelet, I.; Church, M. G. A Logic-Gated Nanorobot for Targeted Transport of Molecular Payloads. *Science* **2012**, *335*, 831–834.

(6) Turner, M.; Golovko, V. B.; Vaughan, O. P. H.; Abdulkin, P.; Berenguer-Murcia, A.; Tikhov, M. S.; Johnson, B. F. G.; Lambert, R. M. Selective Oxidation with Dioxygen by Gold Nanoparticle Catalysts Derived from 55-Atom Clusters. *Nature* **2008**, *454*, 981–984.

(7) Saha, K.; Agasti, S. S.; Kim, C.; Li, X.; Rotello, V. M. Gold Nanoparticles in Chemical and Biological Sensing. *Chem. Rev.* **2012**, *112*, 2739–2779.

(8) Park, J. W.; Shumaker-Parry, J. S. Structural Study of Citrate Layers on Gold Nanoparticles: Role of Intermolecular Interactions in Stabilizing Nanoparticles. *J. Am. Chem. Soc.* **2014**, *136*, 1907–1921.

(9) Park, J. W. Negative-Imaging of Citrate Layers on Gold Nanoparticles by Ligand-Templated Metal Deposition: Revealing Surface Heterogeneity. *Part. Part. Syst. Charact.* **2019**, *36*, 1–9.

(10) Wulandari, P.; Nagahiro, T.; Michioka, K.; Tamada, K.; Ishibashi, K.; Kimura, Y.; Niwano, M. Coordination of Carboxylate on Metal Nanoparticles Characterized by Fourier Transform Infrared Spectroscopy. *Chem. Lett.* **2008**, *37*, 888–889.

(11) Mikhlin, Y. L.; Vorobyev, S. A.; Saikova, S. V; Vishnyakova, E. A.; Romanchenko, A. S.; Zharkov, S. M.; Larichev, Y. V. Applied Surface Science on the Nature of Citrate-Derived Surface Species on Ag Nanoparticles: Insights from X-Ray Photoelectron Spectroscopy. *Appl. Surf. Sci.* **2018**, *427*, 687–694.

(12) Al-Johani, H.; Abou-Hamad, E.; Jedidi, A.; Widdifield, C. M.; Viger-Gravel, J.; Sangaru, S. S.; Gajan, D.; Anjum, D. H.; Ould-Chikh, S.; Hedhili, M. N.; Gurinov, A.; Kelly, M. J.; Eter, M. El; Cavallo, L.; Emsley, L.; Basset, J. M. The Structure and Binding Mode of Citrate in the Stabilization of Gold Nanoparticles. *Nat. Chem.* **2017**, *9*, 890–895.

(13) Munro, C. H.; Smith, W. E.; Garner, M.; Clarkson, J.; White, P. C. Characterization of the Surface of a Citrate-Reduced Colloid Optimized for Use as a Substrate for Surface-Enhanced Resonance Raman-Scattering. *Langmuir* **1995**, *11*, 3712–3720.

(14) Mabuchi, M.; Takenaka, T.; Fijiyoshi, Y.; Uyeda, N. Surface Enhanced Raman Scattering of Citrate Ions Adsorbed on Gold Sol Particles. *Surf. Sci.* **1982**, *119*, 150–158.

(15) Turkevich, J.; Stevenson, P. C.; Hillier, J. A Study of the Nucleation and Growth Processes in the Synthesis of Colloidal Gold. *Discuss. Faraday Soc* **1951**, *11*, 55–75.

(16) Frens, G. Controlled Nucleation for the Regulation of the Particle Size in Monodisperse Gold Suspensions. *Nat. Phys. Sci.* **1973**, *241*, 20–22.

(17) Kasera, S.; Hermann, L. O.; Del Barrio, J.; Baumberg, J. J.; Scherman, O. A. Quantitative Multiplexing with Nano-Self-Assemblies in SERS. *Sci. Rep.* **2014**, *4*, 1–6.

(18) Mahajan, S.; Lee, T.-C.; Biedermann, F.; Hugall, J. T.; Baumberg, J. J.; Scherman, O. A. Raman and SERS Spectroscopy of Cucurbit[n]Urils. *Phys. Chem. Chem. Phys.* **2010**, *12*, 10429–10433.

(19) Benz, F.; Schmidt, M. K.; Dreismann, A.; Chikkaraddy, R.; Zhang, Y.; Demetriadou, A.; Carnegie, C.; Ohadi, H.; Nijs, B. De; Esteban, R.; Aizpurua, J.; Baumberg, J. J. Single-Molecule Optomechanics in “Picocavities.” *Science* **2016**, *354*, 726–730.

(20) Thompson, D.; Liao, J.; Nolan, M.; Quinn, A. J.; Nijhuis, C. A.; Dwyer, C. O.; Nirmalraj, P. N.; Scho, C.; Calame, M. Formation Mechanism of Metal−Molecule−Metal Junctions: Molecule-Assisted Migration on Metal Defects. *J. Phys. Chem. C* **2015**, *119*, 19438–19451.

(21) Hugall, J. T.; Baumberg, J. J.; Mahajan, S. Disentangling the Peak and Background Signals in Surface-Enhanced Raman Scattering. *J. Phys. Chem. C* **2012**, *116*, 6184–6190.

(22) Nara, M.; Torii, H.; Tasumi, M. Correlation between the Vibrational Frequencies of the Carboxylate Group and the Types of Its Coordination to a Metal Ion: An *Ab Initio* Molecular Orbital Study. *J. Phys. Chem.* **1996**, *3654*, 19812–19817.

(23) Larson, D. W.; Lister, M. W. Catalytic Decomposition of Acetonedicarboxylic Acid. *Can. J. Chem.* **1968**, *46*, 823–832.

(24) Hay, B. R. W.; Bond, M. A. Kinetics of the Decarboxylation of Acetoacetic Acid. *Aust. J. Chem.* **1967**, *20*, 1823–1828.

(25) Doyen, M.; Bartik, K.; Bruylants, G. Journal of Colloid and Interface Science UV – Vis and NMR Study of the Formation of Gold Nanoparticles by Citrate Reduction : Observation of Gold – Citrate Aggregates. *J. Colloid Interface Sci.* **2013**, *399*, 1–5.

(26) Lee, Y.; Schade, N. B.; Sun, L.; Fan, J. A.; Bae, D. R.; Mariscal, M. M.; Lee, G.; Capasso, F.; Sacanna, S.; Manoharan, V. N.; Yi, G. Ultrasmooth , Highly Spherical Monocrystalline Gold Particles for Precision Plasmonics. *ACS Nano* **2013**, *7*, 11064–11070.

(27) Li, C.; Shuford, K. L.; Chen, M.; Lee, E. J.; Cho, S. O. A Facile Polyol Route to Uniform Gold Octahedra with Tailorable Size and Their Optical Properties. *ACS Nano* **2008**, *2*, 1760–1769.

(28) Tanaka, N.; Kitano, H.; Ise, N. Raman Spectroscopic Study of Hydrogen Bonding in Aqueous Carboxylic Acid Solutions. 3. Polyacrylic Acid. *Macromolecules* **1991**, *24*, 3017–3019.

(29) Gao, X.; Davies, J. P.; Weaver, M. J. A Test of Surface Selection Rules for Surface-Enhanced Raman Scattering: The Orientation of Adsorbed Benzene and Monosubstituted Benzenes on Gold. *J. Phys. Chem.* **1990**, *94*, 6858–6864.

(30) Company, N. P.; Spencer, N. D.; Lambert, R. M. Chlorine Chemisorption and Surface Chloride Formation on Au(111). *Surf. Sci.* **1981**, *107*, 237–248.

(31) Park, J.; Shumaker-Parry, J. S. Strong Resistance of Citrate Anions on Metal Nanoparticles to Desorption under Thiol Functionalization. *ACS Nano* **2015**, *9*, 1665–1682.

(32) Zhao, L.; Jiang, D.; Cai, Y.; Ji, X.; Xie, R.; Yang, W. Nanoscale Tuning the Size of Gold Nanoparticles in the Citrate Reduction by Chloride Ions. *Nanoscale* **2012**, *4*, 5071–5076.

(33) Gao, P.; Weaver, M. J. Metal-Adsorbate Vibrational Frequencies as a Probe of Surface Bonding: Halides and Pseudohalides at Gold Electrodes. *J. Phys. Chem.* **1986**, *90*, 4057–4063.

(34) Murphy, P. J.; LaGrange, M. S. Raman Spectroscopy of Gold Chloro-Hydroxy Speciation in Fluids at Ambient Temperature and Pressure: A Re-Evaluation of the Effects of PH and Chloride Concentration. *Geochim. Cosmochim. Acta* **1998**, *62*, 3515–3526.

(35) Berman, D.; Krim, J. Impact of Oxygen and Argon Plasma Exposure on the Roughness of Gold Film Surfaces. *Thin Solid Films* **2012**, *520*, 6201–6206.

(36) Martin, R. B. A Complete Ionization Scheme for Citric Acid. *J. Phys. Chem.* **1961**, *1274*, 8–10.

(37) Barrow, S. J.; Kasera, S.; Rowland, M. J.; Del Barrio, J.; Scherman, O. A. Cucurbituril-Based Molecular Recognition. *Chem. Rev.* **2015**, *115*, 12320–12406.

(38) Hay, P. J.; Wadt, W. R. *Ab Initio* Effective Core Potentials for Molecular Calculations . Potentials for the Transition Metal Atoms Sc to Hg. *J. Chem. Phys.* **1985**, *82*, 270–283.

(39) Frisch, M. J.; Trucks, G. W.; Schlegel, H. B.; Scuseria, G. E.; Robb, M. A.; Cheeseman, J. R.; Scalmani, G.; Barone, V.; Petersson, G. A.; Nakatsuji, H.; Li, X.; Caricato, M.; Marenich, A. V.; Bloino, J.; Janesko, B. G.; Gomperts, R.; Mennucci, B.; Hratchian, H. P.; Ortiz, J. V.; Izmaylov, A. F., *et al.* Gaussian 09, revision D.01; Gaussian, Inc.: Wallingford CT, 2016.

(40) C. Le Rue, E.; Etchegoin, P. G. *Principles of Surface-Enhanced Raman Spectroscopy*, 1st ed.; Le Ru, E. C., Etchegoin, P. G., Eds.; Elsevier Ltd: Amsterdam, 2009; pp 474–479.

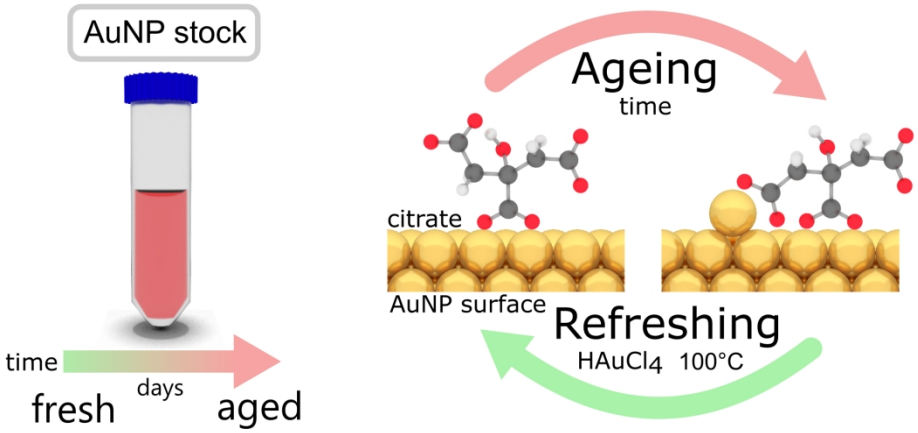
AuNP stock
time
days
fresh
aged
Ageing
time
citrate
AuNP surface
Refreshing
HAuCl4 100°C

TOC